Agro-Industrial Waste as a Source of Raw Material: Eggshell and Ash of Useful for the Synthesis of Hydroxyapatite

Article *in* JOURNAL OF RENEWABLE MATERIALS · January 2022

DOI: 10.32604/jrm.2022.021945

8 authors, including:

Nora Elizondo
Autonomous University of Nuevo León
64 PUBLICATIONS **580** CITATIONS

SEE PROFILE

José de Jesús Quijano-Briones
Autonomous University of Nuevo León
17 PUBLICATIONS **92** CITATIONS

SEE PROFILE

Ernesto Torres López
IHGLIFE
95 PUBLICATIONS **295** CITATIONS

SEE PROFILE

Journal of Renewable Materials

Tech Science Press

DOI: 10.32604/jrm.2022.021945

ARTICLE

Agro-Industrial Waste as a Source of Raw Material: Eggshell and Ash of *Agave salmiana* Useful for the Synthesis of Hydroxyapatite

Nora Elizondo-Villarreal[1,*], Luz H. Verástegui-Dominguez[1], Jose J. Quijano-Briones[1], Francisco J. Vázquez-Rodríguez[2], Eden Rodríguez-Castellanos[3], Enrique López-Cuellar[3], Ernesto Torres-Lopez[1] and Victor M. Castaño-Meneses[4,*]

[1]Universidad Autónoma de Nuevo León, Facultad de Ciencias Físico Matemáticas, Ciudad Universitaria, San Nicolás de los Garza, Nuevo León, México

[2]Universidad Autónoma de Nuevo León, Facultad de Arquitectura, Ciudad Universitaria, San Nicolás de los Garza, Nuevo León, México

[3]Universidad Autónoma de Nuevo León, Facultad de Ingeniería Mecánica y Eléctrica, Ciudad Universitaria, San Nicolás de los Garza, Nuevo León, México

[4]Centro de Física Aplicada y Tecnología Avanzada, Universidad Nacional Autónoma de México, Querétaro, México

[*]Corresponding Authors: Nora Elizondo-Villarreal. Email: nora.elizondovl@uanl.edu.mx; Victor M. Castaño-Meneses. Email: vmcastano@unam.mx

Received: 14 February 2022 Accepted: 24 March 2022

ABSTRACT

Agave salmiana ash and poultry eggshell powder as CaO sources were used for obtaining nanostructured hydroxyapatite (HAP). The synthesis was carried out by the Green Chemistry Hydrothermal Biosynthesis at 180°C with a pH of 5, by reacting CaO from *Agave Salmiana* ash and Eggshell powder, with dibasic calcium phosphate ($CaHPO_4 \bullet 2H_2O$) in an aqueous solution, with *Aloe barbadensis* extract. The product was characterized by X-ray diffraction, Fourier-transform infrared spectroscopy (FT-IR), Scanning Electron Microscopy (SEM), and Transmission Electron Microscopy (TEM). The size and shape of the hydroxyapatite particles changed dramatically in the presence of *Aloe barbadensis*. Large crystals of Hydroxyapatite were observed when Eggshell powder and *Agave salmiana* ash were used as raw materials in the presence of the *Aloe barbadensis* surfactant. Crystals with shapes of ribbons and plates from 1 micrometers to 8 micrometers were observed when using the eggshell powder in the presence of *Aloe barbadensis* and, in the case of *Agave salmiana* ash in the presence of *Aloe barbadensis*, crystals with shapes of quadrangular prisms and hexagonal (polyhedra) with sizes from 2 micrometers to 20 micrometers were observed. Hydroxyapatite was therefore successfully biosynthesized by a green and sustainable method that reduces the environmental impact.

KEYWORDS

Hydroxyapatite; raw materials; *Agave salmiana*; eggshell; *Aloe barbadensis* surfactant

Nomenclature

HAP	Hydroxyapatite
$Ca_{10}(PO_4)_6(OH)_2$	Hydroxyapatite nanoparticles
Ca	Calcium

P	Phosphorus
Å	Angstrom
Ca^{2+}	Ion calcium
PO_4^{3+}	Ion phosphate
Cl^-	Ion chloride
CO_3^{2-}	Ion carbonates
F^-	Ion fluorides
OH^-	Ion hydroxyl
$MgCO_3$	Magnesium carbonate
$CaCO_3$	Calcium carbonate
$CaPO_4$	Calcium phosphate
CaO	Calcium oxide
Kg	Kilogram
SDS	Sodium dodecyl sulfate
CTAB	Hexadecyltrimethylammonium bromide
NaOH	Sodium hydroxide
M	Molar
°C	Celsius degrees
$CaHPO_4$	Dibasic calcium phosphate
pH	Hydrogen potential
h	Hour
rt	Room temperature
XRD	X-ray diffraction
SEM	Scanning electron microscopy
FT-IR	Fourier-transform infrared spectroscopy
Cu	Copper
λ	Lambda
°	Degrees
%	Percent
XRF	X-ray fluorescence
cm	Centimeter
μm	Micrometer
<	Less than

1 Introduction

Hydroxyapatite (HAP) is the main inorganic component of vertebrate bone, representing between 60 and 70% of the calcified human skeleton and 90% of the inorganic bone matrix. The hydroxyapatite nanoparticles ($Ca_{10}(PO_4)_6(OH)_2$ are of great interest for they have a very wide range of applications, from drug delivery and chromatography to gene therapy, and also as a retardant of cancer cells reproduction [1–4]. Hydroxyapatite is an ideal material for artificial bones, as well as a replacement of small parts of bones, dental applications, and bone cement [5–7]. HAP has been found to have an inhibitory function on the growth of many kinds of tumor cells and its nanoparticles have shown stronger anti-cancerous effect than macromolecule microparticles [7,8], and they can improve the adsorption and photocatalytic decomposition of toxic metals, bacteria, viruses and other substances that represent a biological risk [9].

HAP has 39.68% Ca and 18.45% P by theoretical weight, resulting in a molar ratio of Ca/P = 1.67. HAP crystallizes in a hexagonal system with cell values of a = b = 9.432 Å, and c = 6.88 Å. The ionic character of hydroxyapatite allows to partially or completely replace ions from the Ca^{2+}, PO_4^{3+}, OH^- network by others of similar size such as chloride (Cl^-), carbonates (CO_3^{2-}), and fluorides (F^-) resulting in changes in their properties, morphology, solubility, etc. without significant changes in their hexagonal structure [10].

HAP can be synthesized by various methods, such as mechanochemical synthesis, combustion preparation, direct precipitation of aqueous solutions, sol-gel processes, hydrothermal method, emulsion synthesis routes, electrochemical processes, and biomimetics [11–19]. It is known that the mechanochemical and the hydrothermal process allow to produce HAP at nanometric sizes [20,21].

Around 12% of the chicken egg weight is provided by the shell and it is composed of 94% of calcium carbonate ($CaCO_3$), small amounts of magnesium carbonate ($MgCO_3$), calcium phosphate ($CaPO_4$), and organic matter, including mucopolysaccharide-type proteins [22]. Calcium oxide (CaO) is usually produced via the thermal decomposition of limestones obtained through mining and quarrying [23].

Agave belongs to the family of the *Agavaceae* and includes many native species found in the deserts of the American continent. Its leaves are rich in long fibers used to obtain hemp, ropes, and nets, among others products. Agave produces many drinks, among which the most popular are tequila and mezcal, which have been a tradition in Mexico since the seventeenth century. The production of these alcoholic beverages generates an agricultural byproduct in the form of bagasse. For each liter of the mixture, 15 kg of bagasse is produced. Therefore, extensive research has been carried out to use this bagasse produced in arid lands as a renewable energy alternative [24].

In contrast, the *Aloe barbadensis* belongs to a family of more than 200 species called *Aloeneae* of the *Liliaceae* family, originally from Africa, known in the Americas since the 16th century. Around 320 species have been described from the *Aloe* gender. In Mexico, the most frequently cultivated species are *Aloe barbadensis* and *Aloe ferox*, these can be found throughout the country. Currently, there is much interest in the use of *Aloe barbadensis* as a natural surfactant for the synthesis of metal nanoparticles [25].

Accordingly, the aim of this work is the synthesis of hydroxyapatite based on the green chemistry principles, so residues such as eggshells [26] and bagasse from *Agave salmiana* were used as CaO source, as well as *Aloe barbadensis* as a natural surfactant. Their effects on the structure and morphology of HAP were examined.

Some works have demonstrated that a proper selection of biological precursors from sustainable natural resources can effectively replace the commercial surfactant for the fabrication of nanomaterials. The green biotemplate *Aloe barbadensis* plant extract has emerged as a better substitute for industrial surfactant poly (ethylene)glycol for the synthesis of nanomaterials.

The *Aloe barbadensis*-surfactant could provide steric hindrance effects, confining the particle growth to a certain direction. Then, *Aloe barbadensis* a biotemplating/capping agent for the green synthesis of particles. The quantity of surface functional groups from *Aloe barbadensis* allows to control the dynamic characteristics of nucleation and particle growth [27,28].

There are some works were surfactants such as sodium dodecyl sulfate (SDS) and hexadecyltrimethylammonium bromide (CTAB) were used for synthesizing hydroxyapatite, as a regulator of the nucleation and crystal growth, followed by a hydrothermal treatment.

Surfactants are extensively applied to assist and accelerate the hydrothermal reaction process. The surfactants have an effect on the nucleation and growth during the process of aqueous reaction, due to their great solubility in water, low residues, and easy cleaning [29,30].

Our present work represents an innovative and original approach, because we use agro-industrial waste, such as eggshells and *Agave salmiana*, as a source of raw materials, as well as *Aloe barbadensis* as a natural surfactant for the synthesis of hydroxyapatite.

2 Materials and Methods

The green synthesis of Hydroxyapatite (HAP) was carried out by a hydrothermal method in the presence of *Aloe barbadensis* leaf extract. Prior to the synthesis of HAP, the CaO precursor materials were prepared.

2.1 Preparation of Eggshell

The eggshell was washed using distilled water and placed into a 1M NaOH solution for a week, to remove any organic residues. Then, the eggshell was washed again and filtered with distilled water. At 90°C for 12 h, the eggshell was dried before it was milled in a ball mill for 40 min. Then, the $CaCO_3$ powder was obtained from the eggshell by milling and heated at 800°C for 5 h to allow the decomposition of $CaCO_3$ into CaO.

2.2 Preparation of Bagasse Agave salmiana

The bagasse *Agave salmiana* was sun-dried until all the liquid water and alcohols structure were eliminated. Then, the bagasse was burned on direct fire to obtain *ashes* from the bagasse fibers. These fibers contained a high concentration of $CaCO_3$. The bagasse ash from *Agave salmiana* was mechanical milled in a ball mill for 40 min. Finally, ashes of bagasse were heated at 900°C for 3 h to allow the decomposition of $CaCO_3$ into CaO.

2.2.1 Hydroxyapatite Synthesis: Hydrothermal Route

Hydroxyapatite was synthesized by the hydrothermal route with eggshell as CaO source, as described in reference [26].

2.2.2 Hydroxyapatite Synthesis: Hydrothermal Route Using Aloe barbadensis as a Natural Surfactant

Hydroxyapatite was synthesized by the hydrothermal method from commercial dibasic calcium phosphate ($CaHPO_4$) and lime (CaO) obtained from agro-industrial residues (eggshell powder and *Agave salmiana* ash). In a teflon glass, $CaHPO_4$ and CaO were mixed in a 3:1 ratio, then 30% of the mass of the *Aloe barbadensis* extract was added to the mix. The mixture was then acidified with vinegar to a pH of 5 and the teflon glass was sealed. Finally, the vessel is transferred to the reactor and allowed to react at 180°C for 13 h. The obtained powder was filtered and washed with distilled water and dried at 150°C for 2 h.

3 Results and Discussion

The CaO precursors were characterized to determine their composition, size, and morphology, by using XRF and SEM. The products of the green synthesis were characterized by X-ray diffraction, Fourier transform infrared spectroscopy (FTIR), and scanning electron microscopy (SEM). The crystalline phases analysis was performed by powder X-ray diffraction in a Riaku Miniflex II diffractometer with a Cu Kα radiation (λ = 1.5418). The data were collected in an interval of 5°–90° with a scanning speed of 2°/s. For FTIR analysis, an infrared spectrophotometer with an attenuated total reflectance device, Perkin Elmer Spectrum was used. Between 0.1–0.3 g of powder was used for the analysis. The range of wavenumbers to obtain the spectra was 4000–550 cm^{-1}, corresponding to the middle region of the infrared spectrum. The microstructural analysis was carried out using a scanning electron microscope, JEOL JSM-6510LV with EDS detector Oxford Instruments X-Max.

The chemical analysis of the *eggshell* was performed by the volumetric method (atomic absorption) and the technique of X-ray fluorescence (XRF). By atomic absorption a content of Ca = 37.5%, $CaCO_3$ = 93.8%, and Mg = 0.37% was obtained. Table 1 shows the chemical analysis of the eggshell evaluated by X-ray

fluorescence. Fig. 1 shows the microstructure by SEM of the eggshell a) before being processed and b) after the mechanical milling process. From Fig. 1a it can be seen that the eggshell was composed of 12 µm cavities and some areas with organic residues from the eggshell inner shell.

Table 1: Chemical analysis of eggshell and bagasse ash by XRF

Agro-industrial waste	Weight (%)									
Chemical composition	**MgO**	**Al_2O**	**SiO_2**	**P_2O_5**	**SO_3**	**K_2O**	**CaO**	**Fe_2O_3**	**SrO**	**Cl**
Eggshell	0.088	0.045	0.087	0	0.145	0.058	97.421	0.04	0.089	0.027
Agave baggase ash	16.133	0	1.452	3.674	0.762	12.664	64.639	0.239	0.111	0

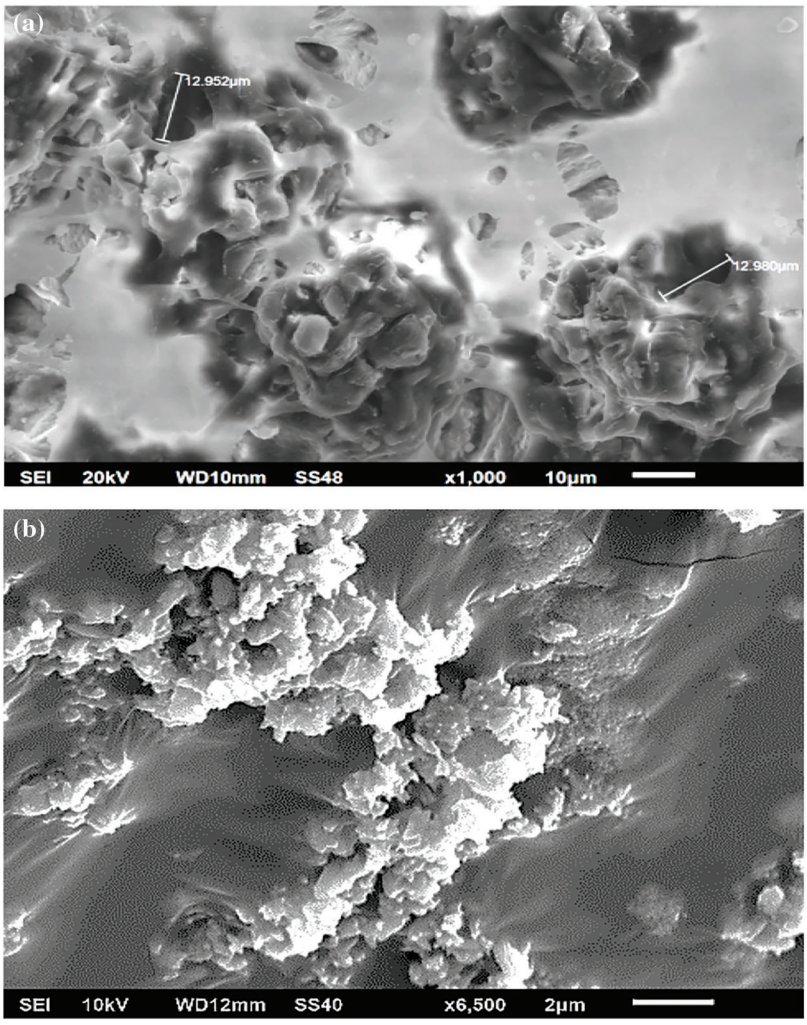

Figure 1: (a) Eggshell surface before the milling process (b) eggshell powder after the mechanical milling process for 40 min

Table 1 shows the chemical analysis of bagasse ash by XRF. Fig. 2 shows the microstructure of the calcined fibers, where irregular particles ($CaCO_3$) are shown with sizes below 2 µm.

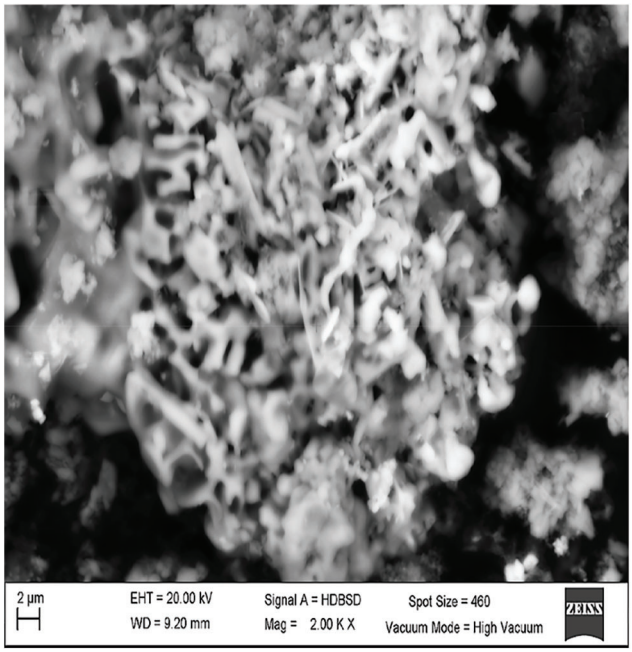

Figure 2: Irregular morphology of the bagasse ash of *Agave salmiana*. The particle size is in the range of 1 to 5 µm

The average particle size (d50) of the eggshell powder was evaluated by a MICROTRAC 3500 size analyzer. An average particle size of d50 < 7 µm was obtained (Fig. 3a).

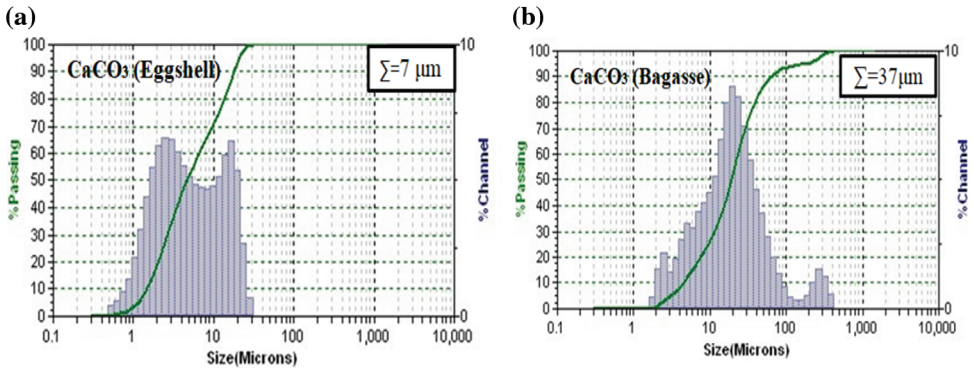

Figure 3: Particle size analyzer MICROTRACT. (a) $CaCO_3$–Eggshell after the milled. (b) $CaCO_3$–*Agave salmiana* bagasse ash after the milled

The average particle size (d50) of the bagasse ash was in the range d50 < 37 µm, as evaluated by a MICROTRAC 3500 size analyzer (Fig. 3b).

After calcination, eggshell, and bagasse ash were characterized by the XRD technique. According to the diffractograms shown in Fig. 4, it can be observed CaO with a cubic structure and spatial group Fm3m, according to Physics and Chemistry of Minerals 27 (1999) 103–111 is the only crystalline phase present after the calcination.

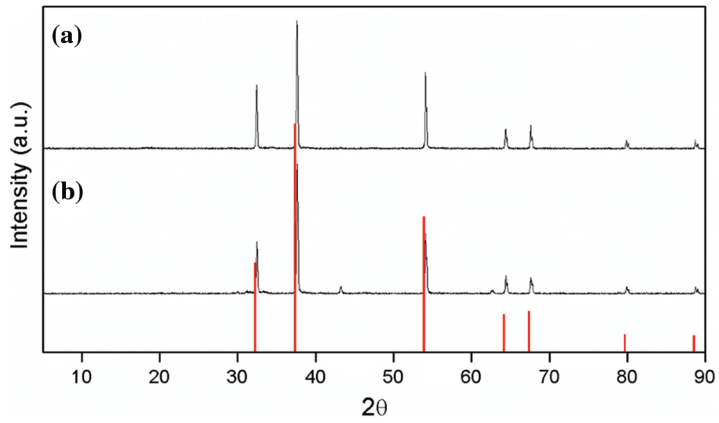

Figure 4: Diffractograms were obtained from calcined (a) eggshell and (b) *Agave salmiana* bagasse ash, and in red color diffraction base pattern of CaO

The resulting powders were synthesized using a) HAP without aloe extract, b) HAP– eggsheell with *Aloe barbadensis extract*, c) HAP–bagasse ash of agave with *Aloe barbadensis* extract, and d) Reference Diffraction pattern. All samples are mainly composed of Hydroxyapatite with a hexagonal structure and spatial group P6_3/m according to American Mineralogist 74 (1989) 870–876. The presence of calcium phosphate acid ($CaHPO_4$) in the synthesized powders was also observed (Fig. 5).

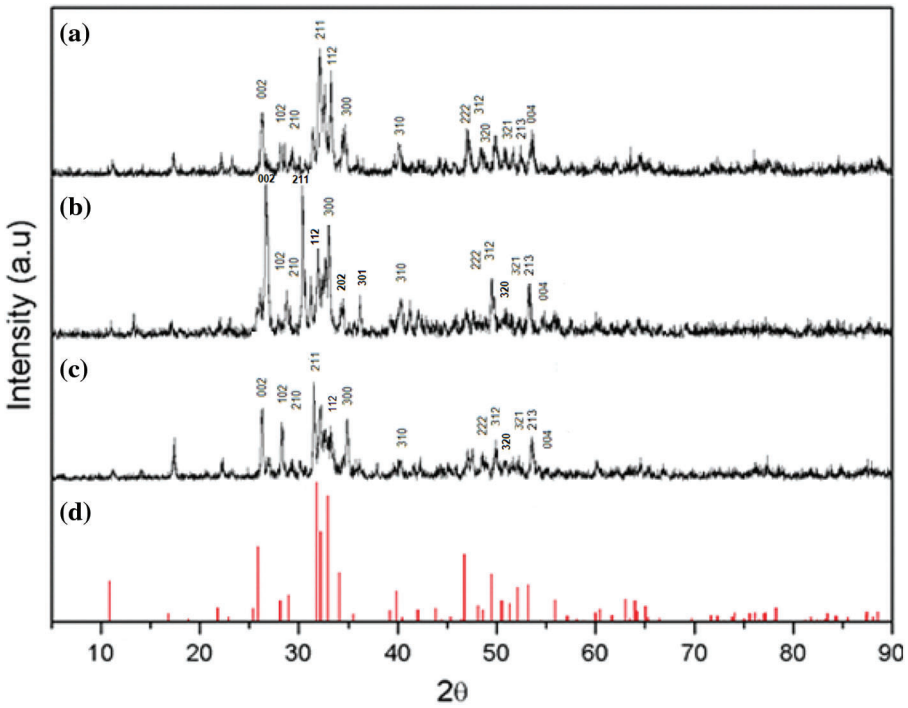

Figure 5: Diffractograms of the Hydroxyapatite synthesis: (a) HAP without aloe extract, (b) HAP–eggshell with *Aloe barbadensis* extract, (c) HAP–*Agave salmiana* bagasse ash with *Aloe barbadensis* extract, and (d) Diffraction base pattern of HAP

The FTIR spectra, Fig. 6, show the characteristic bands for PO_4^{3-} which are observed in 561, 601, 962, 1090 cm^{-1}. The vibration of the OH^- ion is also observed in 631 cm^{-1}. The peak that appears in 875 cm^{-1} corresponds to CO_3^{2-}, 1025 cm^{-1} corresponds to $Ca_3(PO_4)_2$.

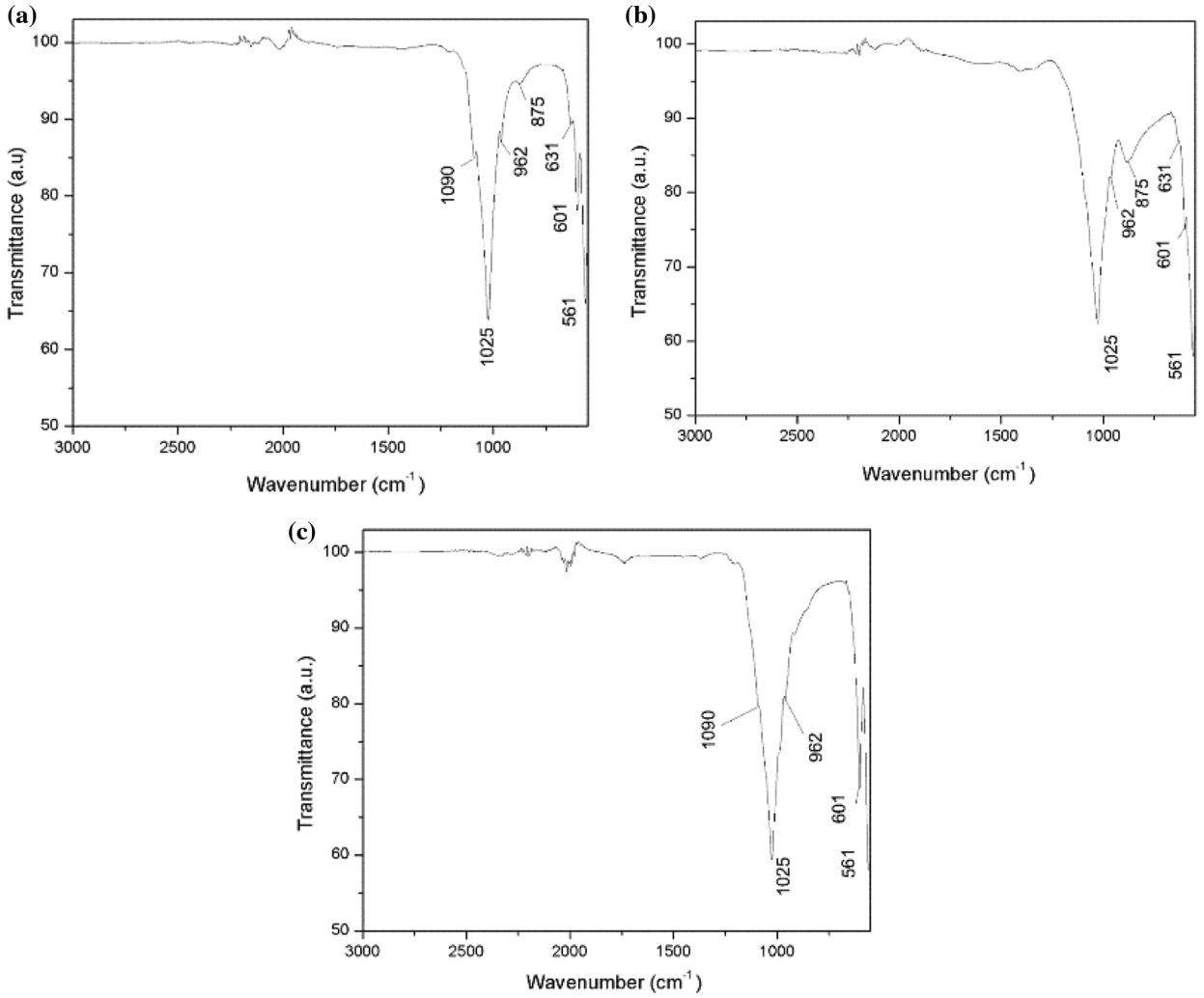

Figure 6: (a) FTIR spectrums of HAP without *Aloe barbadensis* extract. (b) FTIR spectrums of HAP–eggshell using *Aloe barbadensis* extract. (c) FTIR spectrums of HAP–*Agave salmiana* bagasse ash using *Aloe barbadensis* extract

Fig. 7 shows SEM images where it can be seen the morphology of the powder resulting from the hydrothermal synthesis by using CaO obtained from eggshells. Irregular particles of micrometric size are observed but also we can appreciate small needles of nanometric size. Fig. 8 shows SEM images of the HAP morphology by using CaO of eggshell and *Aloe barbadensis*. Rods and some platelets of micrometric size particles are observed. Fig. 9 corresponds to the SEM images of HAP morphology using CaO from *Agave salmiana* and *Aloe barbadensis*. Rectangular and hexagonal rods and some shapeless micrometric size particles are observed. It should be noted that, for each experiment performed, similar particles were obtained with rod and needle morphologies of different dimensions, depending on the

initial conditions used during the synthesis. It is also observed that for the HAP where CaO of eggshell is used, nano-sized particles are generated.

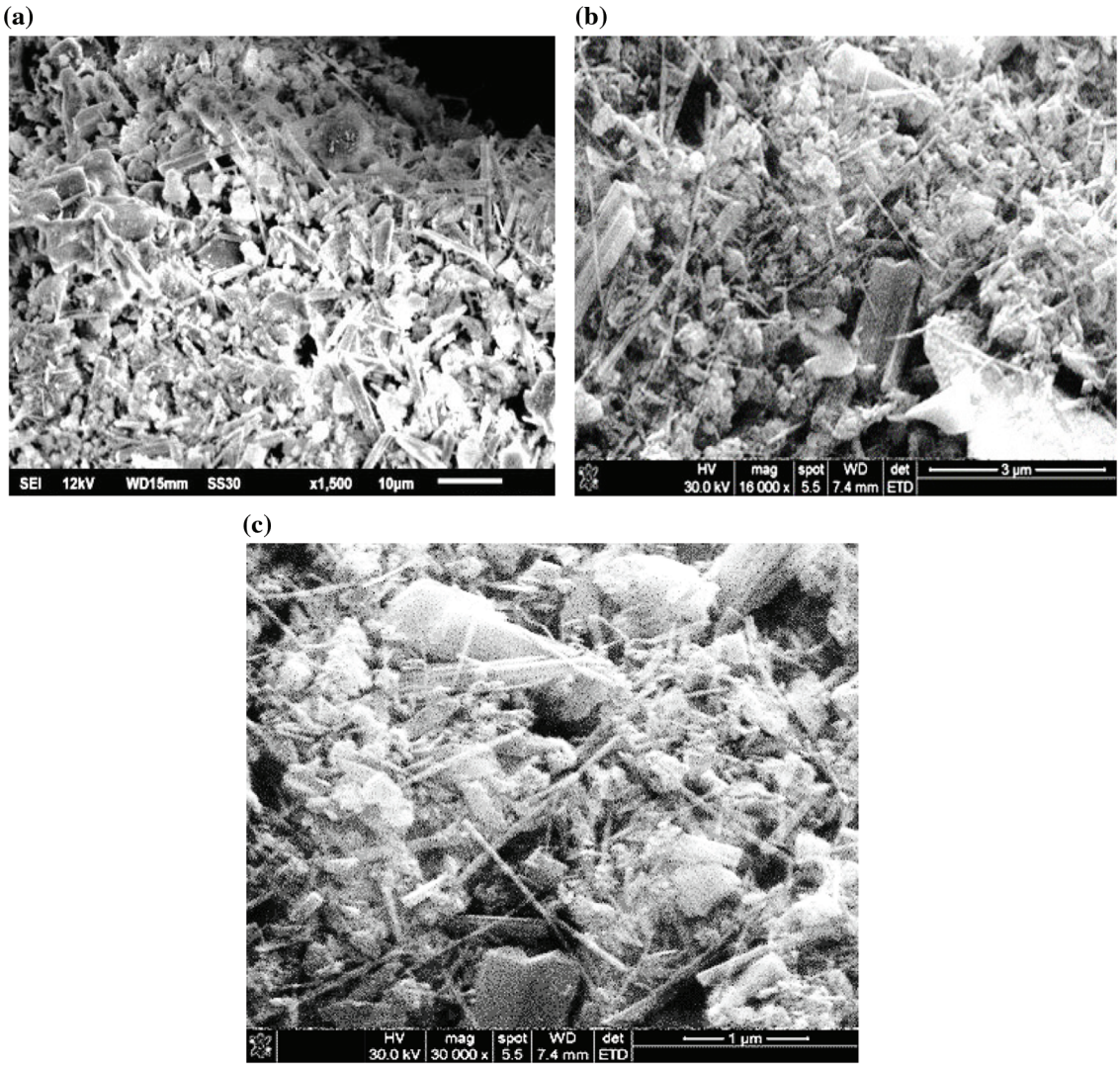

Figure 7: SEM micrographs of hydroxyapatite powder resulting from the hydrothermal synthesis of commercial phosphate and CaO obtained from eggshells with a magnification of (a) 10 µm, (b) 2 µm and (c) 1 µm

Figs. 10a and 10b are TEM images of different zones of the sample of Hydroxyapatite powder resulting from the hydrothermal synthesis with CaO obtained from *Agave salmiana*. As it can be observed, there are several nanograins oriented in different directions. Fig. 11a corresponds to the zoom of Figs. 10a and 11b is the zoom from Fig. 10b, respectively. Interplane distances are indicated in Table 2. Moreover, the expected value of the planes of the Hydroxyapatite and angles between them can be appreciated also in Table 2. As it can be observed, the measured distances are very close to those distances indexed from the expected crystal structure of the Hydroxyapatite. The expected distances were calculated in the CaRIne. Crystallography 3.1 program, introducing the structure of the Hydroxyapatite reported by Ortega et al. [31] and Cao et al. [32].

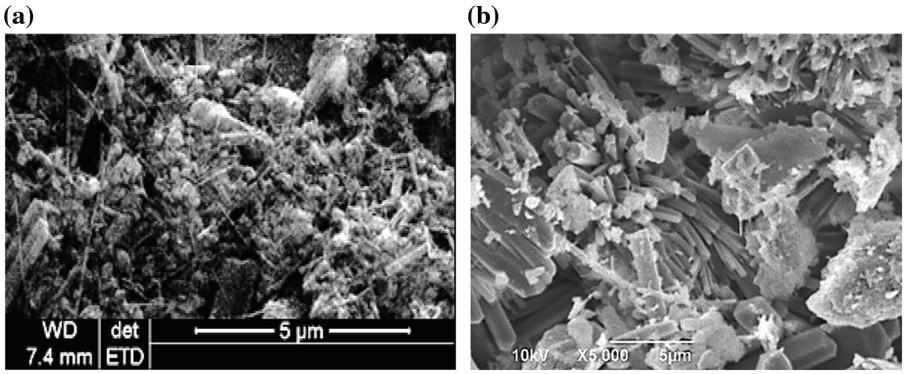

Figure 8: Hydroxyapatite powder micrographs resulting from the hydrothermal synthesis of commercial dibasic phosphate, (a) CaO obtained from eggshells and (b) CaO obtained from eggshells in solution with extract of *Aloe barbadensis*

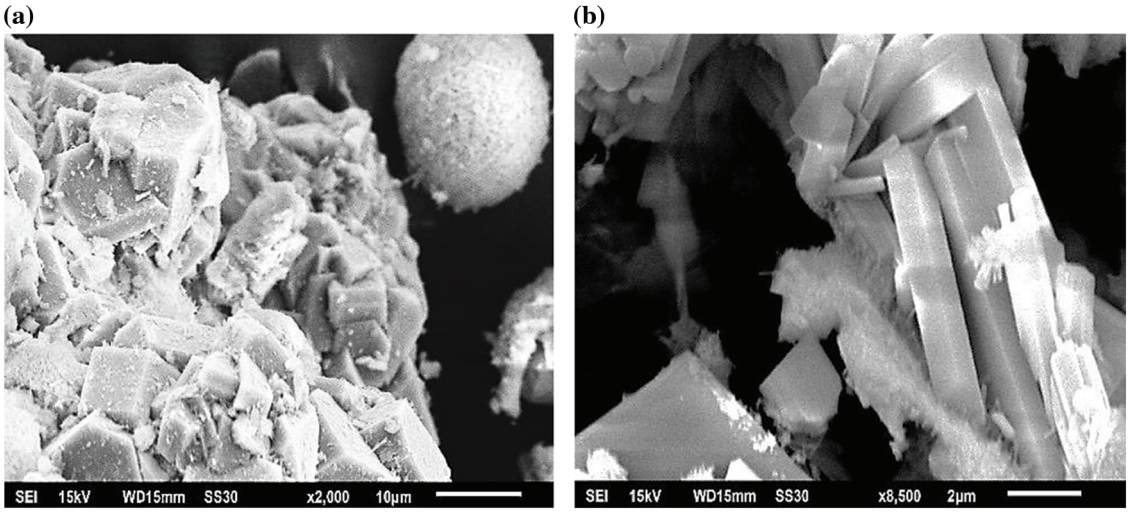

Figure 9: Hydroxyapatite powder micrographs resulting from the hydrothermal synthesis of commercial phosphate, CaO obtained from *Agave salmiana* with a magnification of (a) 10 µm and (b) 2 µm

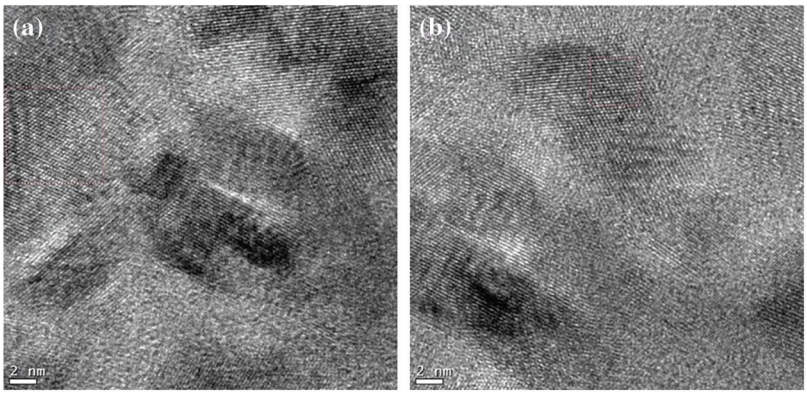

Figure 10: Images in TEM mode in high resolution of the sample of Hydroxyapatite powder resulting from the hydrothermal synthesis of commercial phosphate, CaO obtained from *Agave salmiana* in different zones (a) and (b)

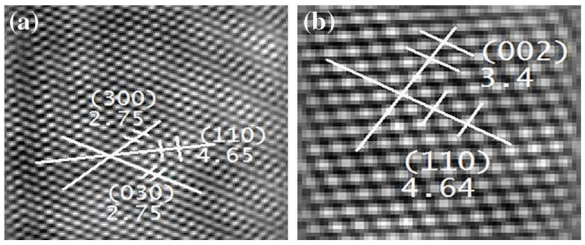

Figure 11: (a) Enlargement of Fig. 10a, to show further microstructure details; (b) Enlargement of Fig. 10b, to show further microstructure details

Table 2: Measured and expected planar distances, indexed planes, and angles between planes of the hydroxyapatite

	d (measured)	d (expected)	Plane	Angle with	Angle with
Fig. 11a	2.75	2.702	(300)	(030) 60°	(110) 30°
Fig. 11a	2.75	2.702	(030)	(300) 60°	(110) 30°
Fig. 11a	4.65	4.68	(110)	(300) 30°	(030) 30°
Fig. 11b	3.4	3.43	(002)	(110) 90°	
Fig. 11b	4.64	4.68	(110)	(002) 90°	

The size and shape of the hydroxyapatite changed dramatically in the presence of *Aloe barbadensis*. Large crystals of Hydroxyapatite were observed when Eggshell powder and *Agave salmiana* ash were used as raw materials in the presence of the *Aloe barbadensis* surfactant. Crystals with shapes of ribbons and plates from 1 micrometer to 8 micrometers were observed when using the eggshell powder in the presence of *Aloe barbadensis* and, in the case of *Agave salmiana* ash in the presence of *Aloe barbadensis*, crystals with shapes of quadrangular prisms and hexagonal (polyhedra) with sizes from 2 micrometers to 20 micrometers were observed.

The *Aloe barbadesis* contain polyphenols, several polysaccharides, and other functional groups. The phenols are highly reactive compounds due to their polydentate ligands with a multiplicity of potential binding sites, i.e., phenolic groups. They may be the active agents in the extracts, responsible for the enhanced stability of micelles and the content of polysaccharides is responsible for the micellization behavior [33,34].

The formation of HAP in the presence of surfactant was accelerated, obtaining large crystals of several micrometers in comparison with HAP synthesized without surfactant at the same reaction time. The added surfactant is then supposed to bind to certain faces of the crystals and bind to certain ions as well so that ions could be incorporated into the existing nuclei at a steady rate and the final shape and size can be well obtained.

The HAP crystals synthesized in the presence of *Aloe barbadesis* exhibited a controlled irregular hexagonal and square prism-like shape and subsequently grew up by the thermal treatment to be larger-sized crystals at a well-dispersed state.

It was also found that the *Aloe barbadesis* surfactant induced heterogeneous nucleation to initiate the nucleation/growth processes.

In contrast, HAP crystals synthesized without surfactant exhibited irregular and nails shaped and aggregated crystals, which are due to dominantly occurring homogeneous nucleation as schematically depicted in Scheme 1 [29–32,34].

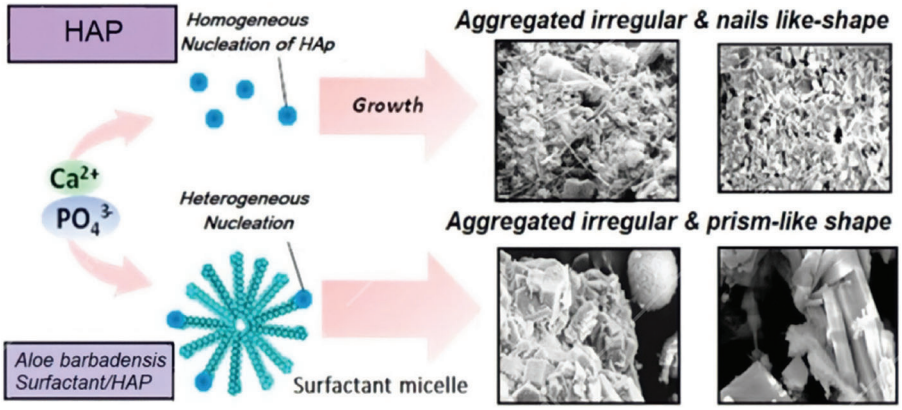

Scheme 1: Illustration of the possible coexistence effect of the *Aloe barbadensis* as a surfactant responsible for the enhanced stability of micelles and for the influence of the micellization behavior on the HAP Crystal Formation Process

4 Conclusions

Hydroxyapatite successfully obtained by a simple hydrothermal method, with Eggshell and *Agave salmiana* as raw materials. The product was a mixture of $CaHPO_4$ and CaO in a ratio of 3:1 with HAP morphology in the form of hexagonal and rectangle prisms, rods, needles, and some platelets. In addition, the use of green chemistry during HAP synthesis with eggshell and *Agave salmiana* using a solution of *Aloe barbadensis* as a surfactant agent, acts as a crystalline growth agent for the particles of HAP.

Acknowledgement: This article is dedicated to the memory of the late Mrs. Aida Meneses-Castillo.

Funding Statement: The funding was provided by Project CE1645-21 PAICYT UANL.

Conflicts of Interest: The authors declare that they have no conflicts of interest to report regarding the present study.

References

1. Ye, F., Guo, H., Zhang, H., He, X. (2010). Polymeric micelle-templated synthesis of hydroxyapatite hollow nanoparticles for a drug delivery system. *Acta Biomaterialia, 6(6),* 2212–2218. DOI 10.1016/j.actbio.2009.12.014.
2. Deppert, W. R., Lukacin, R. (1999). Chapter 5 hydroxyapatite chromatography. In: *Protein liquid chromatography*, pp. 271–299. Amsterdam: Elsevier.
3. Ono, I., Yamashita, T., Jin, H. Y., Ito, Y., Hamada, H. et al. (2004). Combination of porous hydroxyapatite and cationic liposomes as a vector for BMP-2 gene therapy. *Biomaterials, 25(19),* 4709–4718. DOI 10.1016/j.biomaterials.2003.11.038.
4. Roudier, M. P., Vesselle, H., True, L. D., Higano, C. S., Ott, S. M. et al. (2003). Bone histology at autopsy and matched bone scintigraphy findings in patients with hormone refractory prostate cancer: The effect of bisphosphonate therapy on bone scintigraphy results. *Clinical & Experimental Metastasis, 20(2),* 171–180. DOI 10.1023/A:1022627421000.
5. Monma, H., Kamiya, T. (1987). Preparation of hydroxyapatite by the hydrolysis of brushite. *Journal of Materials Science, 22(12),* 4247–4250. DOI 10.1007/BF01132015.
6. Balamurugan, A., Rebelo, A. H., Lemos, A. F., Rocha, J. H., Ventura, J. M. et al. (2008). Suitability evaluation of sol-gel derived si-substituted hydroxyapatite for dental and maxillofacial applications through in vitro osteoblasts response. *Dental Materials, 24(10),* 1374–1380. DOI 10.1016/j.dental.2008.02.017.

7. Ni, G. X., Lu, W. W., Xu, B., Chiu, K. Y., Yang, C. et al. (2006). Interfacial behaviour of strontium-containing hydroxyapatite cement with cancellous and cortical bone. *Biomaterials, 27(29),* 5127–5133. DOI 10.1016/j.biomaterials.2006.05.030.
8. Meena, R., Kesari, K. K., Rani, M., Paulraj, R. (2012). Effects of hydroxyapatite nanoparticles on proliferation and apoptosis of human breast cancer cells (MCF-7). *Journal of Nanoparticles Research, 14(2),* 712. DOI 10.1007/s11051-011-0712-5.
9. Rouhani, P., Taghavinia, N., Rouhani, S. (2010). Rapid growth of hydroxyapatite nanoparticles using ultrasonic irradiation. *Ultrasonics Sonochemistry, 17(5),* 853–856. DOI 10.1016/j.ultsonch.2010.01.010.
10. Brown, P. W., Constantz, B. (1994). *Hydroxyapatite and related materials*. Boca Raton: CRC Press.
11. Kano, J., Zhang, Q., Saito, F., Baron, M., Nzihou, A. (2006). Synthesis of hydroxyapatite with the mechanochemical treatment products of PVC and CaO. *Process Safety and Environmental Protection, 84(4),* 309–312. DOI 10.1205/psep.05175.
12. Tas, A. C. (2000). Combustion synthesis of calcium phosphate bioceramic powders. *Journal of the European Ceramic Society, 20(14–15),* 2389–2394. DOI 10.1016/S0955-2219(00)00129-1.
13. Rodríguez-Clemente, R., López-Macipe, A., Gómez-Morales, J., Torrent-Burgués, J., Castaño, V. M. (1998). Hydroxyapatite precipitation: A case of nucleation-aggregation-agglomeration-growth mechanism. *Journal of the European Ceramic Society, 18(9),* 1351–1356. DOI 10.1016/S0955-2219(98)00064-8.
14. Yoshimura, M., Suda, H., Okamoto, K., Ioku, K. (1994). Hydrothermal synthesis of biocompatible whiskers. *Journal of Materials Science, 29(13),* 3399–3402. DOI 10.1007/BF00352039.
15. Li, Y. B., Groot, K., Wu, J. J., Klein, C. P. A., Meer, S. V. D. (1994). Morphology and composition of nanograde calcium phosphate beedle-like crystal formed by simple hydrothermal treatment. *Journal of Materials Science: Materials in Medicine, 5(6–7),* 326–331. DOI 10.1007/BF00058956.
16. Lim, G. K., Wang, J., Ng, S. C., Gan, L. M. (1999). Nanosized hydroxyapatite powders from microemulsions and emulsions stabilized by a biodegradable surfactant. *Journal of Materials Chemistry, 9(7),* 1635–1639. DOI 10.1039/a809644i.
17. Manso, M., Jimenez, C., Morant, C., Herrero, P., Martınez-Duart, J. M. (2000). Electrodeposition of hydroxyapatite coatings in basic conditions. *Biomaterials, 21(17),* 1755–1761. DOI 10.1016/S0142-9612(00)00061-2.
18. Branda, F., Costantini, A., Luciani, G., Rosso, F., Peluso, G. et al. (2003). Hydroxyapatite coating of polyetrectrolite hydrogels by means of the biomimetric method. *Materials Science and Engineering: C, 23(3),* 367–370. DOI 10.1016/S0928-4931(02)00288-6.
19. Yeon, K. C., Wang, J., Ng, S. C. (2001). Mechanochemical synthesis of nanocrystalline hydroxyapatite from CaO and $CaHPO_4$. *Biomaterials, 22(20),* 2705–2712. DOI 10.1016/s0142-9612(00)00257-x.
20. Wang, A., Yin, H., Liu, D., Wu, H., Wa, D. Y. et al. (2007). Effects of organic modifiers on the size-controlled synthesis of hydroxyapatite nanorods. *Applied Surface Science, 253(6),* 3311–3316. DOI 10.1016/j.apsusc.2006.07.025.
21. Kalyani, G., Rao, G. B., Saradhi, B. V., Kumar, Y. P. (2009). Equilibrium and kinetic studies on biosorption of zinc onto Gallus domesticus shell powder. *ARPN Journal of Engineering and Applied Sciences, 4(1),* 39–49.
22. Mohamad, S. F. S., Mohamad, S., Jemaat, Z. (2016). Study of calcination condition on decomposition of calcium carbonate in waste cockle shell to calcium oxide using thermal gravimetric analysis. *ARPN Journal of Engineering and Applied Sciences, 11(16),* 9917–9921.
23. Chávez-Guerrero, L., Hinojosa, H. (2010). Bagasse from the mezcal industry as an alternative renewable energy produced in arid lands. *Fuel, 89(12),* 4049–4052. DOI 10.1016/j.fuel.2010.07.026.
24. Patel, V. K., Bhattacharya, S. (2013). High-performance nanothermite composites based on aloe-vera-directed CuO nanorods. *ACS Applied Materials & Interfaces, 5(24),* 13364–13374. DOI 10.1021/am404308s.
25. Elizondo-Villarreal, N., Martínez-De-La-Cruz, A., Guerra, R. O., Gómez-Ortega, J. L., Castaño, V. M. et al. (2012). Biomaterials from agricultural waste: Eggshell-based hydroxyapatite. *Water, Air, & Soil Pollution, 223(7),* 3643–3646. DOI 10.1007/s11270-012-1137-1.

26. Patel, V. K., Sundriyal, P., Bhattacharya, S. (2017). Aloe vera *vs*. poly(ethylene)glycol-based synthesis and relative catalytic activity investigations of ZnO nanorods in thermal decomposition of potassium perchlorate. *Particulate Science and Technology, 35(3),* 361–368. DOI 10.1080/02726351.2016.1163299.
27. Patel, V. K., Bhattacharya, S. (2013). High-performance nanothermite composites based on Aloe-Vera-directed CuO nanorods. *ACS Applied Materials & Interfaces, 5(24),* 13364–13374. DOI 10.1021/am404308s.
28. Yan, L., Li, Y., Deng, Z. X., Zhuang, J., Sun, X. (2001). Surfactant-assisted hydrothermal synthesis of hydroxyapatite nanorods. *International Journal of Inorganic Materials, 3(7),* 633–637. DOI 10.1016/S1466-6049(01)00164-7.
29. Wang, Z., Jiang, S., Zhao, Y., Zeng, M. (2019). Synthesis and characterization of hydroxyapatite nano-rods from oyster shell with exogenous surfactants. *Materials Science and Engineering: C, 105(22),* 110102. DOI 10.1016/j.msec.2019.110102.
30. Gomez-Ortega, J. L., Elizondo-Villarreal, N., Guerrero-Villa, H. M. (2004). Visualización cristalográfica de la hidroxiapatita. *Revista de Ingenierías UANL, 7(24),* 46–50.
31. Cao, M., Wang, Y., Guo, C., Qi, Y., Hu, C. W. (2004). Preparation of ultrahigh-aspect-ratio hydroxyapatite nanofibers in reverse micelles under hydrothermal conditions. *Langmuir, 20(4),* 4784–4786. DOI 10.1021/la0498197.
32. Hamman, J. H. (2008). Composition and applications of Aloe vera leaf gel. *Molecules, 13(8),* 1599–1616. DOI 10.3390/molecules13081599.
33. O'Connell, J. E., Fox, P. F. (1999). Effect of extracts of oak (*Quercus petraea*) bark, oak leaves, aloe vera (*Curacao aloe*), coconut shell and wine on the colloidal stability of milk and concentrated milk. *Food Chemistry, 66(1),* 93–96. DOI 10.1016/S0308-8146(98)00248-9.
34. Shiba, K., Motozuka, S., Yamaguchi, T., Ogawa, N., Otsuka, Y. et al. (2016). Effect of cationic surfactant micelles on hydroxyapatite nanocrystal formation: An investigation into the inorganic-organic interfacial interactions. *Crystal Growth & Design, 16(3),* 1463–1471. DOI 10.1021/acs.cgd.5b01599.